February 2003 • NREL/SR-520-33263

Subcontractor Report

Photovoltaic Technologies Beyond the Horizon: Optical Rectenna Solar Cell

Final Report
1 August 2001–30 September 2002

B. Berland
ITN Energy Systems, Inc.
Littleton, Colorado

National Renewable Energy Laboratory

1617 Cole Boulevard
Golden, Colorado 80401-3393

NREL is a U.S. Department of Energy Laboratory
Operated by Midwest Research Institute • Battelle • Bechtel

Contract No. DE-AC36-99-GO10337

February 2003 • NREL/SR-520-33263

Photovoltaic Technologies Beyond the Horizon: Optical Rectenna Solar Cell

Final Report
1 August 2001–30 September 2002

B. Berland
ITN Energy Systems, Inc.
Littleton, Colorado

NREL Technical Monitor: Richard Matson

Prepared under Subcontract No. ACQ-1-30619-11

National Renewable Energy Laboratory

1617 Cole Boulevard
Golden, Colorado 80401-3393

NREL is a U.S. Department of Energy Laboratory
Operated by Midwest Research Institute • Battelle • Bechtel

Contract No. DE-AC36-99-GO10337

NOTICE

Available electronically at http://www.doe.gov/bridge

Available for a processing fee to U.S. Department of Energy
and its contractors, in paper, from:

U.S. Department of Energy
Office of Scientific and Technical Information
P.O. Box 62
Oak Ridge, TN 37831-0062
phone: 865.576.8401
fax: 865.576.5728
email: reports@adonis.osti.gov

Available for sale to the public, in paper, from:

U.S. Department of Commerce
National Technical Information Service
5285 Port Royal Road
Springfield, VA 22161
phone: 800.553.6847
fax: 703.605.6900
email: orders@ntis.fedworld.gov
online ordering: http://www.ntis.gov/ordering.htm

Printed on paper containing at least 50% wastepaper, including 20% postconsumer waste

TABLE OF CONTENTS

Photovoltaic Technologies Beyond the Horizon

Optical Rectenna Solar Cell

1. Background on ITN Energy Systems' Optical Rectenna Technology

1.1. Motivation for Next-Generation, High-Efficiency Solar Cells

Worldwide energy demands have increased by 40% over the last 20 years.[1] Although the deleterious effects of hydrocarbon-based power are becoming increasingly apparent, more than 85% of the world's power is still generated by combustion of fossil fuels.[1] Clean renewable alternative energy sources are required to meet the demands, with direct solar-conversion devices as leading candidates. The worldwide market for conventional photovoltaics (PV) has increased at an annual rate of 20% over the last five years, and industry estimates suggest as much as 18 billion watts per year could ship by 2020.[1] To meet the increased demands for solar-conversion technologies, dramatic improvements are required in state-of-the-art PV technologies. Efficiency improvements and cost/complexity reduction are the main issues that need to be addressed to meet these goals.

Traditional p-n junction solar cells are the most mature of the solar-energy-harvesting technologies. Although great improvements have been made in the last 20 years, energy absorption, carrier generation, and collection are all a function of the materials chemistry and corresponding electronic properties (i.e., bandgap). As a quantum device, the efficiency of PV is a function of, and therefore, ultimately fundamentally limited by, the bandgap and the match of the bandgap to the solar spectrum. For single-junction cells, this sets an upper efficiency limit of ~30%.[2] Even with complex multi-junction designs, the theoretical efficiency plateaus around 55% without excessive concentration of the incident radiation.[3] Current state-of-the-art solar cells are ~20% efficient for single cells and ~30% efficient for multijunction systems.[4] In the long term, the PV industry will require newer, higher efficiency technologies to improve performance and to meet the increasing demands of the solar power market.

As an alternative, ITN Energy Systems is developing next-generation solar cells based on the concepts of an optical rectenna (see Figure 1). ITN's optical rectenna consists of two key elements: 1) an optical antenna to efficiently absorb the incident solar radiation, and 2) a high-frequency metal-insulator-metal (MIM) tunneling diode that rectifies the AC field across the antenna, providing DC power to an external load. The combination of a rectifying diode at the feedpoints of a receiving antenna is often referred to as a rectenna. Rectennas were originally proposed in the 1960s for power transmission by radio waves for remote powering of aircraft for surveillance or communications platforms.[5] Conversion efficiencies greater than 85% have been demonstrated at radio frequencies (efficiency defined as DC power generated divided by RF power incident on the device). Later, concepts were proposed to extend the rectennas into the infrared (IR) and optical region of the electromagnetic spectrum for use as energy collection devices (optical rectennas).[6]

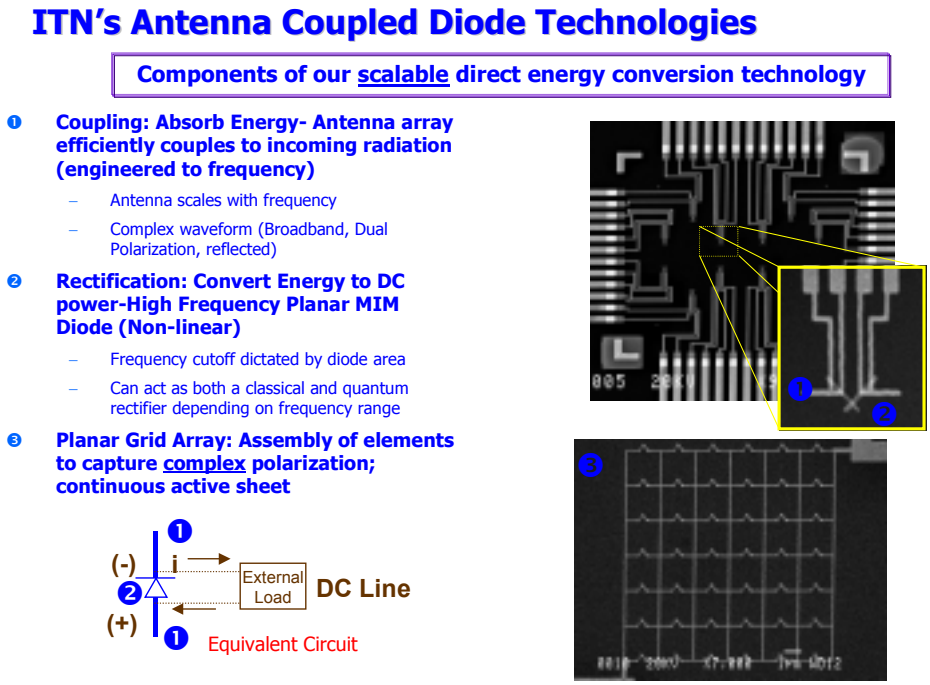

Figure 1. Schematic overview of ITN's optical rectenna.

Early optical rectenna concepts were based on simple scaling of microwave antenna theory, and the proof-of-concept was never demonstrated. Non-optimized element design, impedance mismatch between components, inefficient rectifying junctions, and lack of state-of-the-art nanopatterning may have all contributed to their unsuccessful attempts. In related research programs, ITN has been working extensively in developing antenna arrays with more realistic scaling relationships and more efficient diodes.

Unlike conventional semiconductor-based PV, ITN's optical rectenna is not fundamentally limited, with conversion efficiencies greater than 85% theoretically possible. In fact, ITN has already demonstrated conversion efficiencies greater than 50%, limited only by saturation of the off-the-shelf diodes, using lower-frequency rectenna arrays with wire-bonded Schottky diodes. All aspects of the lower-frequency rectenna arrays are scaleable to the higher THz frequencies required for photovoltaic applications.

1.2. Highlights of ITN's Previous Optical Rectenna Development Effort

In collaboration with researchers at the University of Colorado and the National Institute of Standards and Technology, ITN began developing its optical rectenna technology as part of a DARPA-sponsored effort in energy harvesting. The program focused on both antenna design and validation, as well as on MIM development. Highlights of this past work are summarized to motivate the development plan for the NREL Beyond the Horizons Program.

1.2.1. Antenna Array

As a means for capturing or converting the abundant energy from solar radiation, an antenna is the ideal device because it is an efficient transducer between free space and guided waves. In the case of conventional PV cells, solar radiation is only absorbed if the photon energy is greater than the bandgap. Because the bandgap must also be tuned to minimize the excess energy lost to heat when the photon energy is significantly above the bandgap, a significant portion of the incident solar energy, up to 24%, is not absorbed by conventional PV. In contrast, an adequately designed antenna array can efficiently absorb the entire solar spectrum, with nearly 100% efficiency theoretically possible (efficiencies greater than 96% have been predicted for realistic systems with ITN's models). Rather than generating single electron-hole pairs as in the PV, the electric field (E) from an incident electromagnetic radiation source will induce a time-changing current (i.e., wave of accelerated electric charge) in a conductor. Efficient collection of incident radiation is then dependent on resonance length scales and impedance matching of the antenna to the diode to prevent losses.

In simple microwave antenna theory, the resonant length of the antenna scales linearly with the incident frequency, and in theory the antenna can be scaled to resonate at IR and optical frequencies. However, at IR and optical frequencies, conduction is no longer ohmic, and these simple scaling laws are not accurate. Rather, a majority of the energy in the surface modes is carried in the dielectric above the antenna (often referred to as the skin effect, i.e., surface impedance losses become important). In addition, for solar energy conversion, the antenna must be designed to couple with a fairly complex waveform. The average power per unit area is about 1500 W/m^2, with a maximum intensity at about 0.5 μm. Solar radiation has a moderately broadband electromagnetic frequency spectrum, ranging from a frequency of about 150 THz to about 1,000 THz, corresponding to a free-space wavelength of about 2 μm to about 0.3 μm. Over 85% of the radiation energy is contained in the frequency range from 0.4 μm to 1.6 μm. Efficient antenna/rectifiers, therefore, need to cover a frequency range on the order of 4:1.

Figure 2. Efficiency measurements of a 10 GHz rectenna array with Schottky diodes wire-bonded at the feedpoints of the antenna. Efficiencies > 50 % are demonstrated for relatively large-area arrays (~ 20 cm) and are limited only by saturation of the diodes. Efficiencies approaching 90% are likely with better-quality diodes.

Because the antenna properties scale with wavelength, we were able to demonstrate key aspects of the antenna design and performance as lower frequencies (RF), where fabrication is simpler and commercial diodes can be used. The results show that these arrays can operate at very high efficiencies, > 50%, limited only by saturation of the Schottky diodes (see Figure 2). Because the results in Figure 2 were obtained using inexpensive, standard off-the-shelf Schottky diodes, we expect much higher efficiencies (>85%) could be demonstrated with higher-quality diodes. In addition, we have used the lower-frequency rectenna arrays to address coupling to complex waveforms (elliptical polarization and broadband solar radiation source). Although interference of in-plane DC bus lines and interference effects must be addressed in any design, the grid array, shown in Figure 3, meets all the criteria (i.e., no in-plane interference), with efficiency demonstrations comparable to the linear dipole arrays. These results show that the design of high-absorption-efficiency optical antenna arrays is quite feasible. We will stick with current GRID array designs for feasibility demonstration. Further antenna optimization may be required to reach the ultimate efficiency goals.

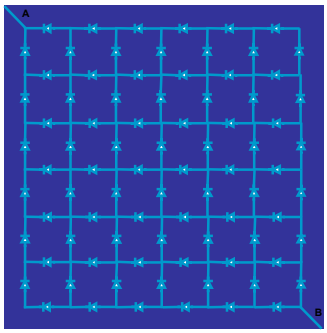

Figure 3. Optimal antenna array design that enables in-plane DC bus lines with minimal coupling, minimized interference between adjacent apertures, and effective coupling to broadband, dual-polarization radiation.

1.2.2. Metal-Insulator-Metal (MIM) diodes

As with the antenna, we must overcome the bandgap limitations of the PV conversion device to achieve high conversion efficiencies. With PV, each photon above the bandgap, regardless of photon energy, generates a single electron-hole pair, which delivers an energy proportional to the bandgap to the load. A photon far above the bandgap still delivers the same energy as a photon exactly matched to the bandgap, with the excess energy lost as heat. In contrast, a sufficiently ideal nonlinear metal-insulator-metal (MIM) diode can circumvent this limitation by operating as an ideal quantum detector in which the voltage at which photogenerated carriers are delivered to the external circuit increases linearly with frequency. The energy delivered to the load can then be as high as the photon energy, for all photon energies.

For high-frequency diodes, the limiting factor is typically parasitic capacitance. Historically, Schottky diodes have been limited to $\nu < 5$ THz, whereas MIM diodes have been used for over 25 years at frequencies down to $\nu \sim 150$ THz (2 μm), currently being extended farther into the IR and optical. State-of-the-art MIM diodes, however, are typically limited by two factors: 1) integration and stability of the point-contact configuration, 2) zero bias response; an external bias is required on most MIMs developed to date to achieve sufficiently ideal diode behavior. Although an external bias may be useful for some applications, it would dramatically reduce the efficiency, and therefore usefulness, in energy-harvesting applications. The key then is to develop planar MIM diodes that are sufficiently non-linear and asymmetric to have good responsivity with no external bias applied.

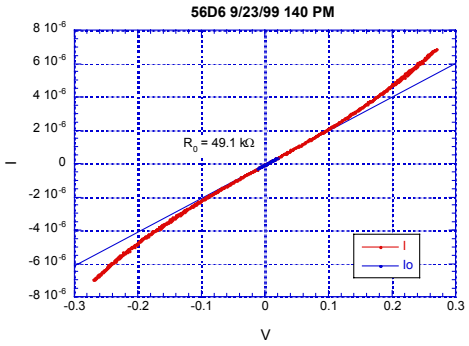

Figure 4. I-V characteristics of a typical nanometer-scale MIM diode. The blue line represents the actual I-V data. The red line is a subtraction of the data from a linear fit to show the slight deviation from a resistor.

The frequency response of the diode is governed by the RC time constant. Because the impedance of the device must be relatively close to the impedance of the antenna (~180 ohms), the capacitance must be minimized for operation at THz frequencies. To achieve the attofarad capacitance (10^{-18}) required, device areas less than 100 nm by 100 nm are required for typical material systems. ITN, in collaboration with NIST, was able to successfully fabricate the small diode areas with devices that generated DC power when illuminated with IR radiation. Unfortunately, the current-voltage (I-V) characteristics of typical devices were not highly nonlinear or asymmetric. The poor I-V characteristics prevented us from showing attractive conversion efficiencies.

In parallel, ITN and NIST were developing micron-sized MIM diodes to optimize processing of the devices. Figure 5 shows the I-V characteristic for a good Cr/CrOx/Au device. Notice that the micron-scale device shows significantly higher nonlinearity, slight asymmetry, and lower zero-bias impedance. To show efficient solar-energy harvesting, we will need to achieve I-V characteristics similar to the micron-scale devices at the nanometer-length scales. In addition, the micron-scale devices require additional optimization (i.e., lower impedance, higher nonlinearity).

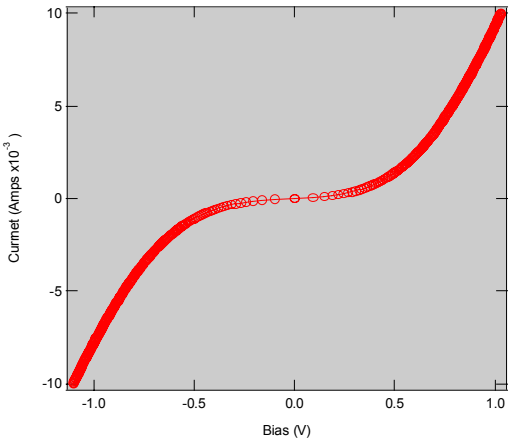

Figure 5 I-V characteristic of a good micron-scale MIM diode (Cr/CrOx/Au).

The efficiency of the MIM diodes was evaluated using a coplanar waveguide test fixture (Figure 6). An AC waveform could be fed to the diode using the coplanar waveguide, thereby eliminating efficiency losses due to inefficient free-space coupling (impedance mismatch at waveguide/diode interface can still lead to significant losses). Using these structures, we were able to measure conversion efficiencies ~0.1% at low frequencies (MHz). We believe that much of the incident radiation was reflected at the waveguide (50 ohm)/diode (~10,000 ohm) interface. In addition, the devices were fairly symmetric. Asymmetry improvements should improve the efficiency considerably. As a result, we identified diode optimization and scaling to nanometer-length scales as the key development necessary to show feasibility of this promising technology.

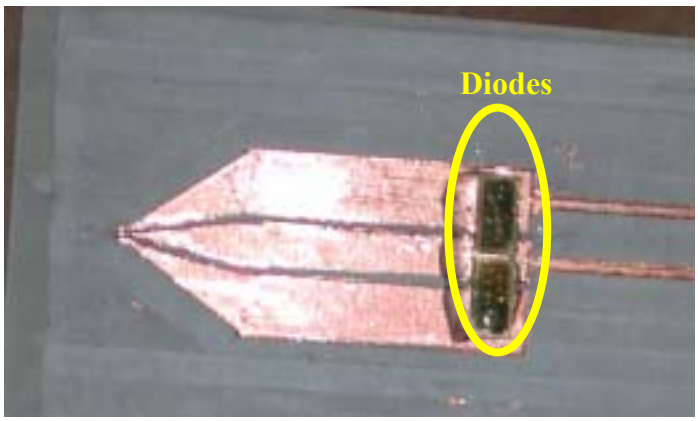

Figure 6. Picture of coplanar waveguides with MIM diodes wire-bonded for efficiency testing.

1.3. Approach/Objectives for the Photovoltaic Technologies Beyond the Horizons Program

As discussed above, the key challenge remaining is to develop the diode technology. The Beyond the Horizons project focused on optimization of a tunneling diode structure, incorporation into a rectenna array, and demonstration of proof-of-principle. Based on the 0.1% conversion-efficiency measurements of the previous program, we thought that low single-digit conversion efficiencies may be possible by optimizing the diode characteristics at the nanometer-length scales (i.e., achieve diode characteristics at nanometer-length scales similar to the performance already demonstrated at micron-length scales). A three-tiered development effort was identified-starting with discrete diode optimization and ending with demonstrated performance at a single frequency in the solar spectrum. The key development efforts are as follows:

- *Optimization of a discrete nanopatterned diode:* Develop fabrication process using ion-beam deposition that leads to controlled and reproducible fabrication of nanopatterned diodes with desired dark I-V characteristics. The ion-beam deposition system enables a controlled microstructure, leading to better uniformity and control of the MIM tunneling barrier composition and thickness, as well as interface integrity and stability (i.e., minimized surface states, impurity incorporation, etc).

- *Fabricate a single rectenna element:* Optimized discrete diode structures will be monolithically integrated into single rectenna elements for operation at a single rectenna frequency.

- *Demonstrate technical feasibility:* Show efficient energy harvesting at a single frequency in the solar spectrum, including current and voltage generated by illumination with a single wavelength.

2. Results/Discussion

As discussed in section 1, significant progress had been made in related research efforts to establish confidence that optical antennas can be designed and fabricated to efficiently match to the broadband, arbitrarily polarized nature of the solar spectrum. In addition, patterning techniques had been established to allow monolithic integration of the MIM diodes into the antenna array. The main challenge remained the fabrication of MIM diodes with sufficient nonlinearity, asymmetry, and low impedance. As a result, the majority of the program research focused on the optimization of discrete nanopatterned diodes. In particular, we focused on the development of ion-beam deposition techniques to enable better control of film microstructure, as well as plasma oxidation for the formation of controlled barrier layers. Diodes with promising performance characteristics would then be incorporated into antenna arrays for light I-V response testing.

2.1. Task 1: Optimization of discrete nanopatterned diode

High-efficiency solar-energy harvesting requires the device to be operated with no external bias. Therefore, the optimized device must be highly nonlinear and highly asymmetric, with a low turn-on voltage with low impedance that is matched to the antenna aperture. Based on ITN's models developed in previous programs, we had identified Nb/NbOx/M diodes, where M represents the counter-electrode materials such as Nb, Ag, or Au, as a good candidate for feasibility demonstrations. Previous development, however, relied on electron-beam evaporation and nascent oxide barrier formation that resulted in poor uniformity and reproducibility of the barrier formation, making a systematic optimization of device performance impossible. For the Beyond the Horizons program, we fabricated MIM diodes using ion-beam deposition to address these issues. The ion-beam system is equipped with an ion gun for deposition, an additional gun for ion milling, and reactive RF plasma processing. These capabilities should allow for improved control of film microstructure and plasma oxidation as a more reliable barrier formation technique.

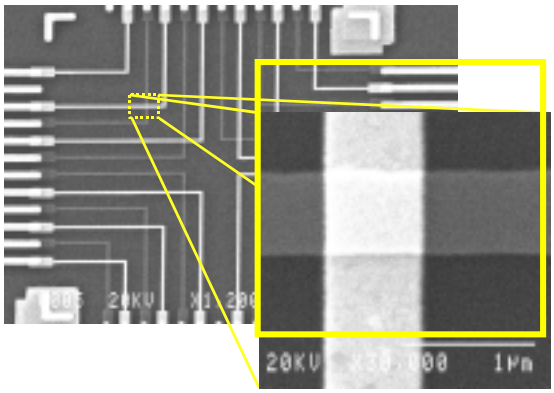

Figure 7. SEM image of the crossing wire pattern. The area where the two wires cross defines the MIM diode.

As shown in Figure 7, our MIM diodes are fabricated as two metallic wires separated by an ultra-thin tunneling barrier. The active device area is defined by the overlap of the two wires. The base metal electrodes are fabricated using e-beam lithography and lift-off techniques. Using the ion beam to deposit the niobium, we have achieved thin-film resistivities on the order of 70 μΩ-cm, compared to resistivities >200 μΩ-cm observed with electron-beam evaporation. In addition, the Nb films were evaluated at the NREL characterization laboratory with the help of Glenn Teeter and Dr. Sally Asher using X-ray photoelectron spectroscopy (XPS). The XPS results showed impurity levels (i.e., carbon, oxygen, and other trace impurities) below the detection limits of the instrument.

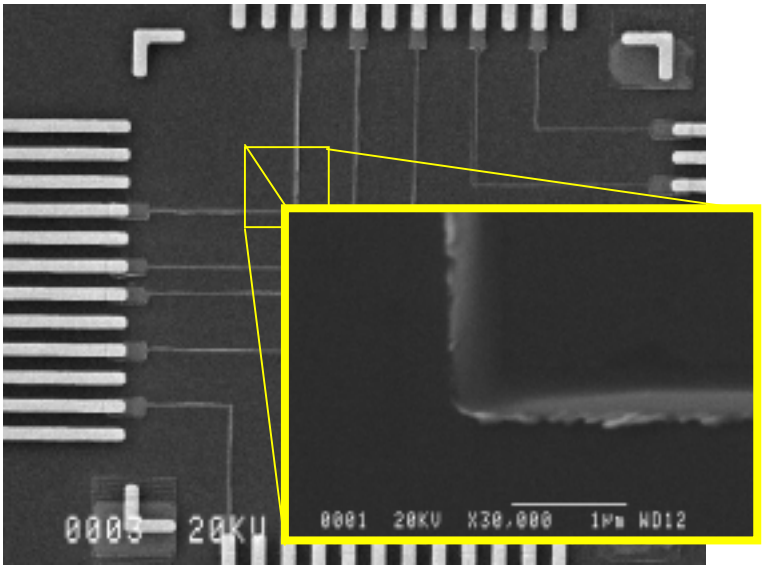

Figure 8. SEM image of Nb base metal electrodes deposited in the ion-beam system. Notice the formation of jagged edges that degrade device performance.

Figure 8 shows that although the ion-beam system is improving the resistivity, it has also led to poor edge definition during "lift-off." Metal wires that were deposited in the ion-beam system exhibited large amounts of edge debris that led to poor contact resistance with subsequently deposited layers. Although "lift-off" techniques are in general prone to ripping, leading to jagged edges, the large distribution of incident angles for depositing atoms in ion-beam deposition exaggerates this problem. We believe the problem may also be related to the energetics of the deposition. Ion-beam systems typically operate at relatively high energy (2-20 eV), compared to e-beam evaporation that is a relatively low-energy deposition technique (<0.5 eV). Therefore, in ion-beam systems, the incident atoms potentially have enough energy to sputter material off a growing film and to redeposit nearby. Although edge debris can dramatically effect device performance, this problem can be mitigated by using a CO_2 snow clean after Nb deposition. Although further optimization of the ion-beam deposition is required, the snow clean has proven to be effective for the formation of MIM test structures to optimize barrier formation.

Once we achieved uniform and reproducible fabrication of the metal electrodes, we shifted our attention to the barrier formation and optimization. To overcome the inherent limitations of nascent oxide barriers, we switched to a plasma oxidation process. The tunneling barrier layer is formed by exposure of the base metal electrode to an O_2/Ar plasma environment. Barrier formation was studied as a function of oxygen partial pressure, oxidation time, deposition temperature, and as a function of stage rotation. With the help of Glenn Teeter at NREL, we processed NbOx films for XPS analysis of the stoichiometry. Figure 9 shows the XPS spectrum for a typical plasma-formed tunneling barrier. Only peaks for the desired barrier, Nb_2O_5, and the underlying Nb metal were observed. This indicates that suboxides of Nb, such as NbO and Nb_2O, which are conducting rather than insulating, are not present in significant quantities.

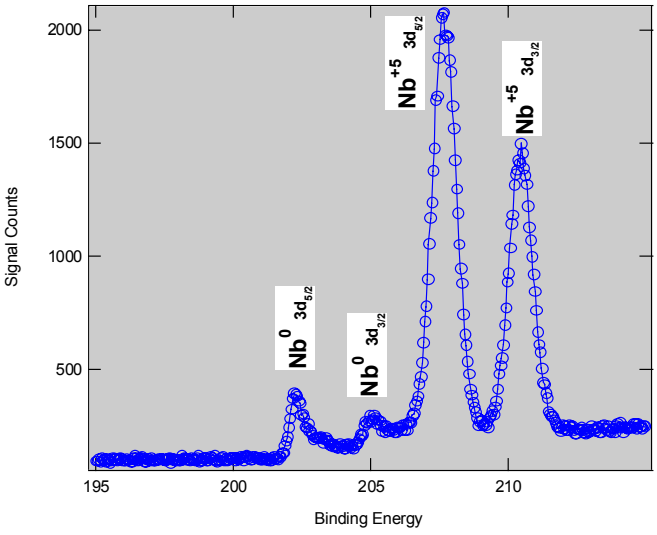

Figure 9. XPS spectrum of NbOx tunneling barrier.

Using similar processing conditions, we made Nb/NbOx/Nb tunneling diodes. Diode characteristics were studied as a function of overlap area, as well as process conditions. Because we had only achieved reasonable diode characteristics with micron-size diodes in past programs, we began with relatively large diode areas (500 nm x 500 nm). The ion-beam processing enabled dramatic improvements in the diode characteristics at nm-length scales. Diode characteristics observed only with micron-size devices in the previous programs were now routinely achieved with nanometer-scale devices. Figure 10 shows the I-V characteristic of all diodes on a typical chip. Of the ten possible devices on this chip, eight of them yielded diodes with similar I-V responses and zero-bias resistance (ZBR). Compared to the diodes that were fabricated with a nascent oxide, the plasma oxide devices have a much lower impedance (~2 kΩ) due to the ability to form much thinner barrier layers. More importantly, the devices were much more uniform across the chip (ZBR ranged from 0.5-2.5 kΩ, compared to 70 kΩ-20 MΩ for nascent barriers). In addition, the typical I-V curve is highly nonlinear (NL=7 at 0.3 V) and has a low

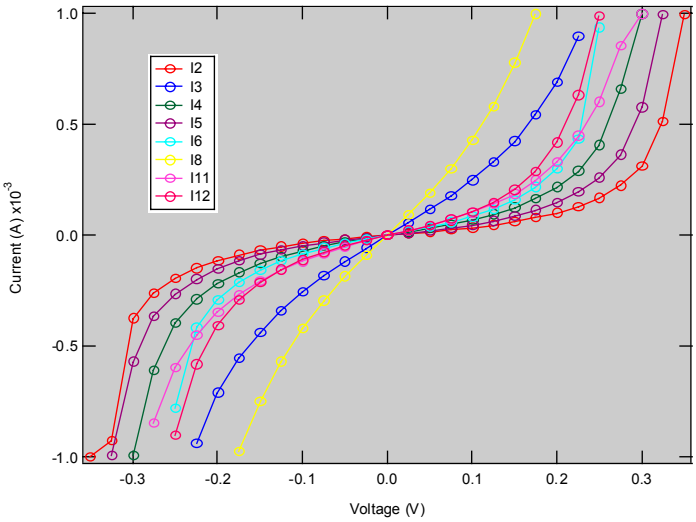

Figure 10. I-V characteristics for Nb/NbOx/Nb diodes.

turn-on voltage (~200 mV). These particular diodes are still relatively large (500 nm x 500 nm) to respond at higher frequencies.

A target diode active area of 100 nm x 100 nm is required for energy harvesting. The target of 100 nm x 100 nm was chosen based on literature reports for MIM diodes used for IR detection operating at 10 microns, the target wavelength of the current program, and first-order capacitance estimates based on handbook values for the materials. Over the course of the program, we slowly decreased the active area of the devices from 500 nm x 500 nm to 100 nm x 100 nm. Typical diode curves as a function of device area are shown in Figure 11.

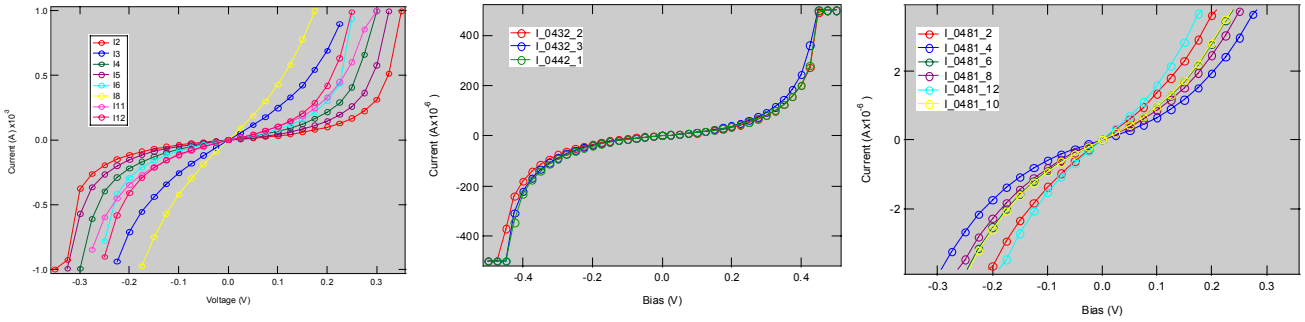

500 nm x 500 nm **225 nm x 225 nm** **100 nm x 100 nm**

Figure 11. Dark I-V characteristics of typical MIM diodes as a function of the active device area.

For comparison, we show the performance scaling of devices prior to the start of the current program. As can be seen in Figure 12, the devices at the micron scale were very good prior to the current program. However, the nanometer devices were more like resistors than diodes. Furthermore, there were 12 diodes on a single chip (process run). The resistance of the nanometer devices often varied over a few orders of magnitude on a single chip. Whatever good results we achieved were random and required several runs to get a high enough sampling to get a few good devices.

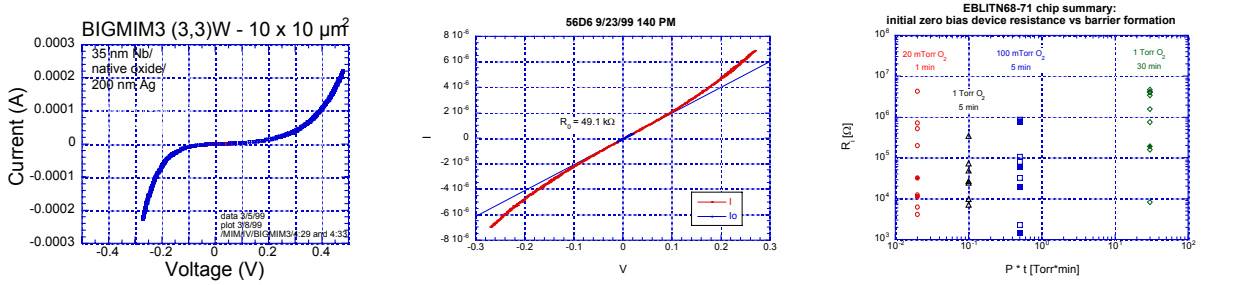

10 μm x 10 μm **50 nm x 50 nm** **Resistance Spread Across Chips**

Figure 12. Typical diode characteristics as a function of device area for devices fabricated using electron-beam evaporation and nascent or thermal oxide tunneling barriers as part of previous programs for a 10-micron device (left), a 50-nm device (right), and the resistance spread across a give chip 50 nm devices (right-each color represents one chip).

The performance of the devices was evaluated based on nonlinearity (NL), impedance, and uniformity and reproducibility of the fabrication. The nonlinearity is defined as dI/dV*V/I and is equal to 1 for a resistor. As a rough estimate, nonlinearity greater than 3 should be sufficient to expect measurable conversion efficiencies. The impedance of the device should ideally be matched to the antenna, typically on the order of a few hundred ohms. Finally, the devices should be uniform across a chip and reproducible from chip to chip. As shown in Figure 4, we have demonstrated diodes with promising characteristics. Typical diodes exhibited nonlinearity greater than 3. Figure 13 shows that typical devices have relatively low impedance (order of tens of kilo-ohms) and the improved uniformity achieved in the current program. A good chip exhibited greater than 80% yield, with less than 20% variation across a chip. Chip-to-chip reproducibility was on the order of 25% (one out of every four chips would meet these specifications).

Although we are encouraged by the improvements during the current program, there are still several aspects of the diode that require additional optimization. As mentioned, the impedance of the devices was still too high. Although the ion-beam processing improved uniformity and reproducibility greatly, the control and systematic variation of device performance were still not achieved. Further optimization of the plasma oxidation process would likely enable better control. However, due to time limitations, we were unable to complete the optimization. The process used to achieve diode characteristics such as those shown in Figure 11 and Figure 13 was then used to fabricate and test single rectenna elements.

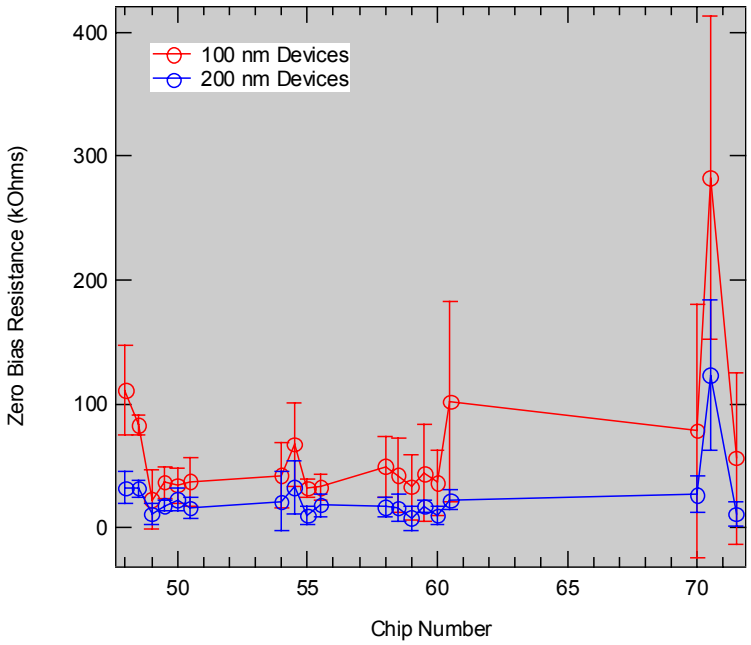

Figure 13. MIM diode impedance as a function of chip number for several runs near the end of the program. The impedance is shown for both 100- and 200-nm devices.

It is also worth noting that the devices fabricated are still highly symmetric. We attempted to fabricate Nb/NbOx/Au diodes to promote asymmetry in the device characteristic required for high-efficiency energy harvesting. Unfortunately, these devices were much less reproducible than Nb/NbOx/Nb devices shown above, and, therefore, difficult to incorporate into antenna arrays. Because we have observed power generation with symmetric diode curves in the past, we chose to pursue feasibility demonstration with the Nb/Nb diodes and come back to optimize asymmetry in future efforts.

2.2. Task 2: Fabrication a single rectenna

The objective of the program was to demonstrate the feasibility of the proposed approach at a single wavelength in the solar spectrum. As shown in Figure 14, the standard terrestrial solar spectrum does not have significant power density above ~2-3 microns. However, because ITN's optical rectenna is an antenna-based technology that scales with wavelength, we have chosen to focus on a feasibility demonstration at 10 microns, where most of the previous patterning technologies were established. Efficient conversion at 10 microns effectively demonstrates the feasibility of the concepts at shorter wavelengths in the solar spectrum. In addition, the demonstration at a single frequency required only a single-dipole antenna. We, however, chose to use the broadband grid array that is more representative of the ultimate optical rectenna. As demonstrated with the RF analog, the grid array has a broadband response (4:1 bandwidth demonstrated previously) and couples effectively to arbitrarily polarized light. Given the target test wavelength of 10 microns, the grid array was designed to couple to broadband IR centered at 30 THz (10 μm) and should respond to roughly 4-16-micron radiation based on the RF analog. Diode areas of 100 nm x 100 nm were chosen for fast IR response time.

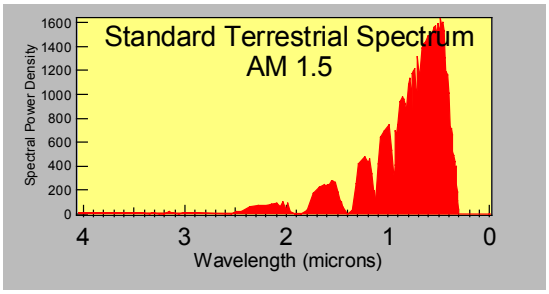

Figure 14. Standard AM1.5 solar spectrum.

Using the diode processing schemes defined in Task 1, we fabricated grid arrays with monolithically integrated MIM diodes. Figure 15 shows an SEM image of the grid array. It is worth noting that the grid array, as shown schematically in Figure 3, is only a half-wave rectifier. Two grid arrays placed back to back and rotated 90 degrees relative to one another would be required to achieve full-wave rectification. As expected, experience from previous programs with monolithic integration was easily translated to the current program. All 36 diodes were perfectly aligned with antenna elements.

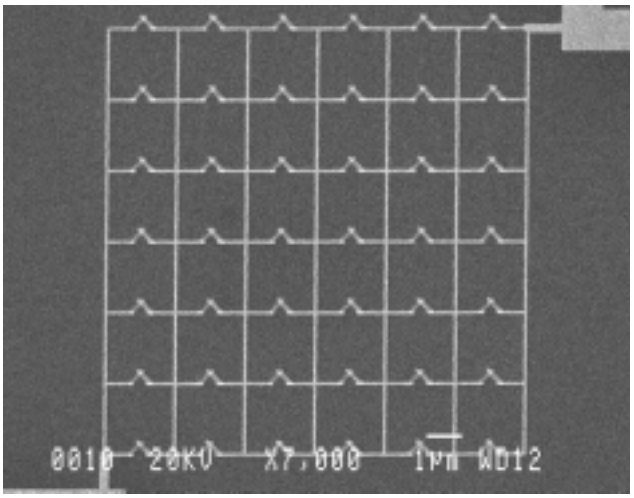

Figure 15. SEM image of a single rectenna element.

The dark I-V characteristics of the grid array were characterized. As shown in Figure 16, the I-V response is reasonably nonlinear, but highly symmetric. As with the discrete diodes, the impedance is still higher than desired, but lower than those demonstrated in previous programs. As discussed above, nonlinearity was used for discrete diodes to measure deviation from a resistor required to achieve rectification. A more accurate predictor of performance is the classical responsivity, defined as the second derivative of the I-V curve divided by the first derivative. The rectified voltage is then directly proportional to the classical responsivity and the optical power of the incident wave. The classical responsivity is then a function of the operating bias (voltage) of the device. For energy harvesting, we require high responsivity near zero bias. Models from previous programs predicted high conversion efficiency if the responsivity of the diode approaches 7 A/W. Our current grids have a sensitivity of ~1 A/W at bias (~500 mV), but drops off closer to zero bias. These devices were then used for illuminated I-V testing to measure conversion efficiency.

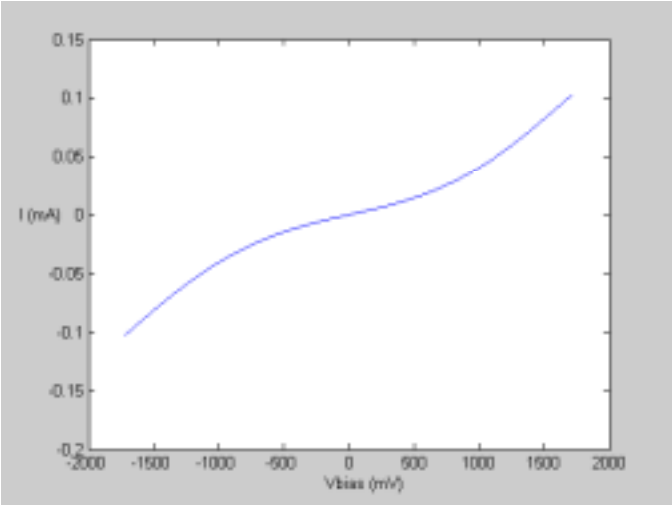

Figure 16. Dark I-V characteristic for a grid array with monolithically integrated MIM diodes.

2.3. Task 3: Demonstrate Technical Feasibility

The conversion efficiency was measured using CO_2 laser illumination (30 THz). Figure 17 shows the rectified voltage (μV) as a function of incident optical power (mV). (Note that all measurements of the grid array light and dark I-V were performed at the University of Central Florida in the Laboratory of Professor Glenn Boreman by his graduate students at no charge to the contract. We are grateful for their help in characterizing our devices.) As expected, DC power was generated upon illumination. Note that the x-axis denotes optical power incident on a power meter with diameter of 25 microns (an area of 4.9 x 10^{-6} cm^2). The approximate aperture area of the grid is 100 microns squared, or about a factor of 5 lower. Therefore, the illumination on the grid is about a factor of five lower than that shown (i.e., 8 mW on the x-axis corresponds to ~325 W/cm^2 on the grid; actual power coupled into the diode is much less; see notes below). Unfortunately, the efficiency of the device is still quite low, much less than 1% (efficiency defined as DC power out/IR optical power in). There are several reasons we believe the efficiency is still low, even though we have made dramatic improvements in the diode characteristics over the last year.

A significant loss occurs in the coupling efficiency of the free-space radiation into the antenna. Although our previous models predict that greater than 95% of the free-space radiation can be coupled in the antenna, even at THz frequencies, the higher-frequency radiation requires additional design modification to achieve these results. Standard antenna designs used to demonstrate high efficiency in the RF yield only ~0.1%-1% coupling at 30 THz. Therefore, although we are shining ~325 W/cm^2 on the grid, only 325 mW/ cm^2-3.25 W/cm^2 are coupled into the antenna. In collaboration with researchers at University of Central Florida, we have a road map to modify antenna materials and design to optimize this coupling, and we expect to see a dramatic increase (a few orders of magnitude) in efficiency if successful.

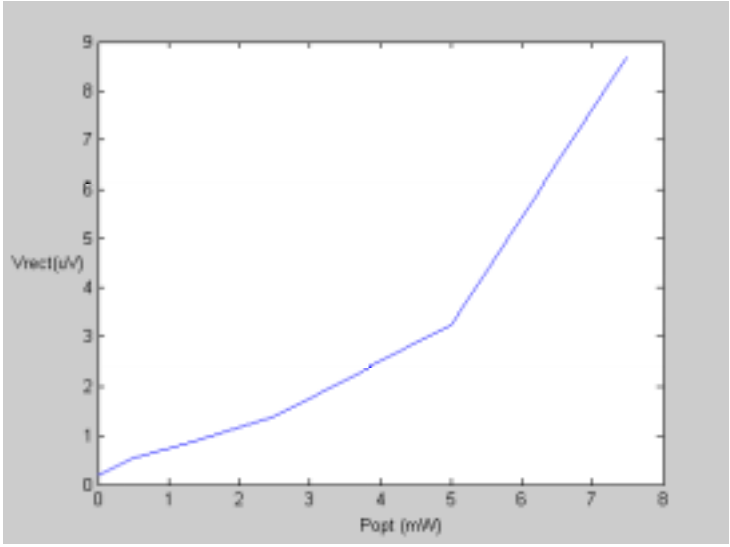

Figure 17. Optical response of the grid array (rectified voltage as a function of optical power).

Another significant loss occurs due to the impedance mismatch at the antenna diode interface. Based on rough estimates of our antenna design, the impedance of the antenna is ~100 ohms, whereas, the diode impedance is >10,000 ohms. Using a rough estimate based on voltage standing wave ratios, only ~1%-2% of the antenna energy is coupled into the diode. Collectively, the coupling efficiency loss and the impedance mismatch result in a power coupled in the diode of only 3.25-30.25 mW/cm^2. This is significantly less than the solar energy at AM1.5 (100 mW/cm^2). The efficiency of the diode is a function of the driving power (as is shown in the figure), so higher efficiency is expected at the AM1.5 flux. Although we have made good progress in reducing the impedance of highly nonlinear diodes in the current program, we know there is still quite a bit of room for reduced barrier thickness, higher integrity interfaces, etc., that should lead to better impedance matching and better coupling into the diode. The impedance of the diode also has an effect on the frequency response of the diode, which is basically set by the RC time constant of the device. Our choice of 100 nm x 100 nm diodes is based on lower impedance devices. Therefore, the cutoff frequency of these particular devices is probably >30 THz. Although the devices still respond at 30 THz, the parasitic capacitance dramatically lowers efficiency. Again, improvements in barrier thickness, etc., should dramatically improve this efficiency.

In addition, all measurements were performed at an external load impedance of 1,000 ohms. This is not likely to be the optimal load for this particular array, but we only had limited external loads available in the current set-up. If we tested these devices as a function of load, we would likely see an improvement in efficiency. The symmetric nature of the MIM diodes also limits efficiency. To show this, we have measured efficiency of the device operated at zero bias and

slightly below the knee of the diode curve (the use of external bias effectively adds asymmetry to the diode). The efficiency at bias was a factor of 40 greater than the unbiased efficiency. Again, solving the interface wetting and other materials/process issues to enable two metal electrodes with different work functions should lead to higher-efficiency conversion. Finally, although these diode characteristics are considerably better than those fabricated prior to the program, our models show there is still significant room for improvement (e.g., we should be able to achieve higher sensitivity—approaching 10 A/W—and shift the voltage scale of the nonlinearity closer to zero bias).

3. Summary

We have observed tremendous improvements in discrete diode fabrication and characteristics over the course of the program. Prior to this program, nanodiode fabrication could best be described as a hit-or-miss approach, where several runs were needed in the hopes of getting one or two devices. In addition, the devices fell into two general categories: (1) very high impedance (>5 MOhm) and high nonlinearity, or (2) very low nonlinearity (basically resistors—only very slight deviation from a line) and lower impedance (~2,000 ohms). With improvements during the Beyond the Horizons program, we were routinely getting diodes with both high nonlinearity and lower impedance (~10,000 ohms). We also observed several promising device characteristics, such as a high responsivity (~1 A/W at 500 mV). Although the reproducibility of the devices improved, our ability to systematically control diode characteristics still needs improvements. As a result, the diodes used to show feasibility typically are higher impedance than required. Also, the devices are still symmetric in nature. Future work to have better control over the tunneling barrier formation and the ability to use metal electrodes of different work functions is required to bring this technology to true feasibility demonstration.

As expected, once the device characteristics were improved, we were able to incorporate the diodes into single rectenna elements relatively easily using procedures established in previous programs. We have chosen our grid array as the single rectenna element for its broadband frequency response and response to elliptically polarized light. The single rectennas were designed for the spectral region from ~4-16 microns centered at 10 microns. Due to the scalable nature of antenna-based technologies, the lessons learned from this approach are directly relevant to higher frequencies required to match to the solar spectrum.

Unfortunately, when these grid arrays were tested with a CO_2 laser, we learned that the device performance is still far from our goal of single-digit conversion efficiencies defined at the beginning of the program. As outlined above, we have identified several reasons for the low conversion efficiency. None of these limitations are related to fundamental physical limits that can not be overcome with process/materials improvements and improvements in testing procedures. We feel that we have developed a good understanding of the basic materials properties that need to be tweaked (i.e., thinner barriers, better controlled interfaces) and have identified ion-beam processing as a flexible approach to tuning these properties to be able meet these goals in future efforts. Therefore, we still believe that the remaining issues can be solved and that the optical rectenna still has tremendous potential for solar-energy harvesting.

Major Reports Published: None

Major Articles Published:

"Optical Rectenna for Direct Conversion of Sunlight to Electricity," B. Berland, L. Simpson, T. Collins, and B. Lanning, NCPV Program Review Proceeding, p:323-4 (2001).

Acknowledgements:

We would like to thank the NREL Photovoltaic Technologies Beyond the Horizons program for the support of this research effort. We would also like to thank Dr. Sally Asher and Glenn Teeter of the NREL characterization labs for their support in analyzing the tunneling barrier formation with XPS, and Keith Emery of the NREL cell and modular measurement team for his thoughts on device characterization and efficiency testing. Finally, we would like to thank Professor Glenn Boreman's laboratory at the University of Central Florida for their support in grid array characterization, both light and dark I-V.

---

[1] The National Photovoltaics Program Plan 2000-2004, Photovoltaics–Energy for the New Millennium, DOE/GO-10099-940 (Jan 2000).

[2] W. Shockley and H. Queisser, *Journal of Applied Physics,* vol. 32, 510 (1961).

[3] C.H. Henry, *Journal of Applied Physics,* vol. 51, 4494 (1980).

[4] M.A. Green, K. Emery, D.L. King, and S. Igari, *Progress in Photovoltaics: Research and Applications*, vol. 8, 187 (2000).

[5] W.C. Brown, *IEEE Transactions on Microwave Theory and Techniques,* vol. MTT-32, 1230 (1984).

[6] A.M Marks, U.S. Patent No. 4445050 (1984), B.J. Zwan, U.S. Patent No. 4251679 (1981).

REPORT DOCUMENTATION PAGE

Form Approved
OMB NO. 0704-0188

1. AGENCY USE ONLY (Leave blank)	2. REPORT DATE	3. REPORT TYPE AND DATES COVERED
	February 2003	Final Report 1 August 2001 – 30 September 2002

4. TITLE AND SUBTITLE
Photovoltaic Technologies Beyond the Horizon: Optical Rectenna Solar Cell, Final Report, 1 August 2001 – 30 September 2002

5. FUNDING NUMBERS
PVP32601
ACQ-1-30619-11

6. AUTHOR(S)
B. Berland

7. PERFORMING ORGANIZATION NAME(S) AND ADDRESS(ES)
ITN Energy Systems, Inc.
8130 Shaffer Parkway
Littleton, Colorado 80127-4107

8. PERFORMING ORGANIZATION REPORT NUMBER

9. SPONSORING/MONITORING AGENCY NAME(S) AND ADDRESS(ES)
National Renewable Energy Laboratory
1617 Cole Blvd.
Golden, CO 80401-3393

10. SPONSORING/MONITORING AGENCY REPORT NUMBER
NREL/SR-520-33263

11. SUPPLEMENTARY NOTES
NREL Technical Monitor: Richard Matson

12a. DISTRIBUTION/AVAILABILITY STATEMENT
National Technical Information Service
U.S. Department of Commerce
5285 Port Royal Road
Springfield, VA 22161

12b. DISTRIBUTION CODE

13. ABSTRACT *(Maximum 200 words)*: ITN Energy Systems is developing next-generation solar cells based on the concepts of an optical rectenna. ITN's optical rectenna consists of two key elements: 1) an optical antenna to efficiently absorb the incident solar radiation, and 2) a high-frequency metal-insulator-metal (MIM) tunneling diode that rectifies the AC field across the antenna, providing DC power to an external load. The combination of a rectifying diode at the feedpoints of a receiving antenna is often referred to as a rectenna. Rectennas were originally proposed in the 1960s for power transmission by radio waves for remote powering of aircraft for surveillance or communications platforms. Conversion efficiencies greater than 85% have been demonstrated at radio frequencies (efficiency defined as DC power generated divided by RF power incident on the device). Later, concepts were proposed to extend the rectennas into the IR and optical region of the electromagnetic spectrum for use as energy collection devices (optical rectennas).

14. SUBJECT TERMS: PV; solar conversion technology; optical rectenna solar cell; free-space wavelength; broadband electromagnetic frequency spectrum; metal-insulator-metal (MIM); nanopatterned diode; electron beam evaporation;

15. NUMBER OF PAGES

16. PRICE CODE

17. SECURITY CLASSIFICATION OF REPORT	18. SECURITY CLASSIFICATION OF THIS PAGE	19. SECURITY CLASSIFICATION OF ABSTRACT	20. LIMITATION OF ABSTRACT
Unclassified	Unclassified	Unclassified	UL